

Vehicle Brake vibrations at very low driving velocities

Wolfgang Seemann Hartmut Hetzler

seemann@itm.uni-karlsruhe.de

Abstract

Vibrations in vehicle brake systems have been subject to research for a long time. One simple phenomenological model is the classical friction oscillator, consisting of a mass on a belt.

A closer look to a real brake system reveals that from the tyre's contact on the street to the disc the brake torque is transmitted via the tyre, which also possesses elastic, dissipative and inertial properties. Motivated by this fact an extended 2-DOF friction oscillator model is developed featuring the rim's inertia and the dissipative and elastic behaviour of the tyre.

In this article the model is given and simulation results are presented. By means of spectral density analysis these data are examined and it is found, that additional torsional elasticity and damping can induce very low frequent vibrations in the regime of low driving velocities, that cannot be observed using the classical mass-on-a-belt-model. An analytical stability analysis of the steady state is performed and stability maps over system parameters and the friction characteristic's slope are given.

In addition an outlook on further studies is given.

1 Model

Mechanical Modell

The model consists of two identical masses m which are pressed onto a disc (moment of inertia J) by the brake force F_B . The disc is connected to a ring by a torsional damper d_1 and spring c_1 . The mass m is connected to the car by a spring c_2 and a damper d_2 . Herein the masses m represent the brake pads and partially the moved mass of the saddle (as a "reduced mass"), the disc represents the brake disc and the rim and finally the ring stands for the tyre's tread. The elastic and dissipative elements c_1 , d_1 are introduced in order to model the behaviour of the rubber tyre by means of a linearized tyre model [1]. The system is assumed to be symmetric, so the coordinate x describes the position of both pads, further φ is the angle of the disc and ψ ($\dot{\psi} = const$) the angle of the tread. The latter is given by kinematics as

$$\dot{\psi} = \frac{v_{car}}{r}. \quad (1)$$

with the kinematic stiction condition. In both approaches it is supposed, that the sliding friction force is linearly coupled to the normal force by a coefficient μ which depends only on the relative velocity between the sliding partners.

With μ as the sliding friction coefficient, μ_0 the sticking friction coefficient and λ the constrained force in the sticking case, the friction force is given by

$$R = \begin{cases} \min(\lambda, \mu_0 N) : v_{rel} = 0 \\ \mu N \operatorname{sign}(v_{rel}) : v_{rel} \neq 0 \end{cases} \quad \text{with } \mu = \begin{cases} \text{const} : \text{Coulomb} \\ f(v_{rel}) : \text{Stribeck} \end{cases} . \quad (7)$$

In the sticking case $v_{rel} = 0$ the number of DOF reduces from two to one and the system's motion is constrained by the kinematic sticking condition and its holonomic constraint equation

$$0 = v_{rel} = b(\dot{\alpha} + \dot{\psi}) - \dot{x} \quad (\dot{\psi} = \text{const}) \quad \rightarrow \quad 0 = b(\alpha + \psi) - x + C_0, \quad (8)$$

wherein C_0 represents the initial conditions at the onset of sticking. The constraint force λ is determined as Lagrange multiplier introducing (8) into the equations of motion (2). While with the Coulomb characteristic μ is constant, the Stribeck

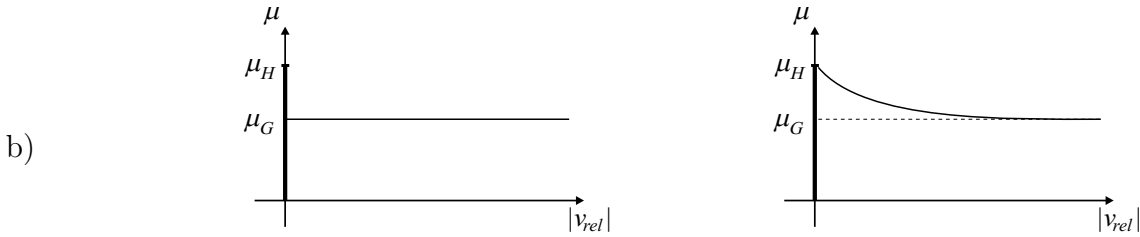


Figure 2: a) Coulomb Friction – b) Stribeck Friction

characteristic is for low relative velocities approximated by

$$\mu = (\mu_H - \mu_G) \exp(-|v_{rel}|c_\mu) + \mu_G \quad (9)$$

with a slope parameter $c_\mu < 0$.

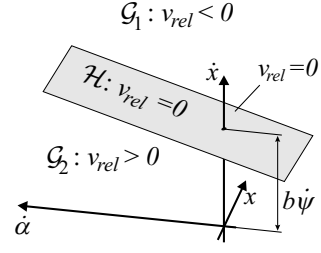
Within our work, a structure switching technique was used to deal with the change between sticking and sliding friction. As long as $|v_{rel}| > 0$ holds the sliding friction is determined using either Coulomb's or Stribeck's friction characteristic as $R = \mu N$. In this sliding friction regime (2) is applied for simulation. When $|v_{rel}| = 0$ occurs the friction forces is determined as a constraint force λ . If this constraint force doesn't exceed the maximum of $R_{max} = \mu_0 N$, sticking holds, therefore the number of DOF reduces to one and (3) is used for simulation. This latter equation contains the kinematic constraint implicitly.

2 Phase-space und simulated limit cycles

Since the number of dimensions exceeds three, only subspaces of the four dimensional state space can be plotted. In order to visualize the stick-condition (8) the subspace $(x, \dot{x}, \dot{\alpha})$ is chosen. In this subspace (8) describes a plane \mathcal{H} whose position

is determined by the parameter $\dot{\psi}$, since $(0, 0, b\dot{\psi})$ is the point where the \dot{x} -axis traverses the plane.

Below this plane the contact point on the disk is faster than that on the pad ($v_{rel} > 0$, semispace \mathcal{G}_2), above it is slower (semispace \mathcal{G}_1). Since the energy flows from the disk to the pads, the pads cannot be faster than the contact point on the disk and so possible system states are to be expected either in the plane \mathcal{H} or in the below semispace.



The system has three possible types of attractor: a steady state point, a limit cycle (which may be periodic or quasiperiodic) and a chaotic attractor. If the system starts in a point of the phase space and doesn't reach the stick plane \mathcal{H} , no energy is brought into the system and dissipation causes the system to end up in the steady state, if the latter is stable (cf. chapter 4). For Stribeck friction the steady state point may be repelling causing the system to move towards the limit cycle. With $\dot{\psi} > 0$ the steady state point is in the $(x, \dot{x}, \dot{\alpha})$ -subspace on the positive x -axis, with $\dot{\psi} < 0$ on the negative x -axis.

If the system's state reaches \mathcal{H} , self-excited vibrations can come up, which are sustained by the energy added during stiction (i.e. motion in \mathcal{H}) and lead into a limit cycle or a chaotic attractor.

Figure 3 and 4 shows limit cycles for Coulomb friction characteristic for two different driving velocities. Obviously the system's behaviour changes radically when the car speed is lowered. For sufficiently low $\dot{\psi}$, the simple limit cycle bifurcates in a complex limit cycle or chaotic attractor featuring extended motion in the α and $\dot{\alpha}$ coordinate.

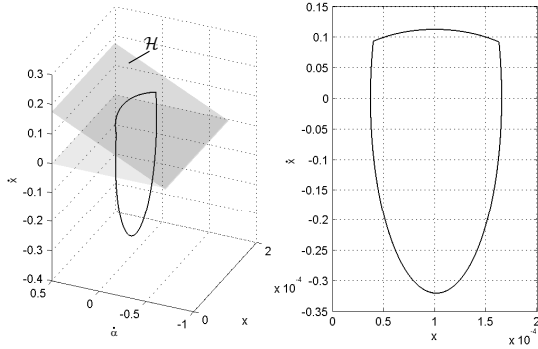


Figure 3: Phase subspace with stick condition plane \mathcal{H} . Limit cycle for $v_{car} = 0.2m/s$

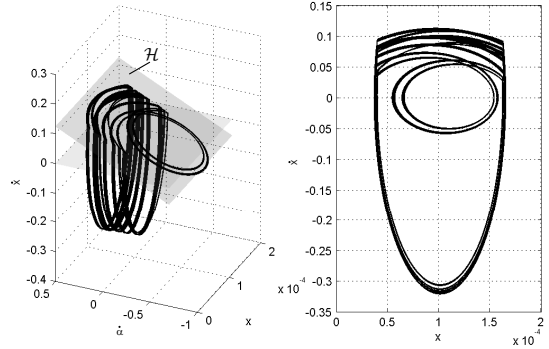


Figure 4: Phase subspace with stick condition plane \mathcal{H} . Limit cycle for $v_{car} = 0.1m/s$

3 Spectral power density analysis

Spectral power density analysis was carried out in order to identify the dominating frequencies and to classify the type of attractor [4].

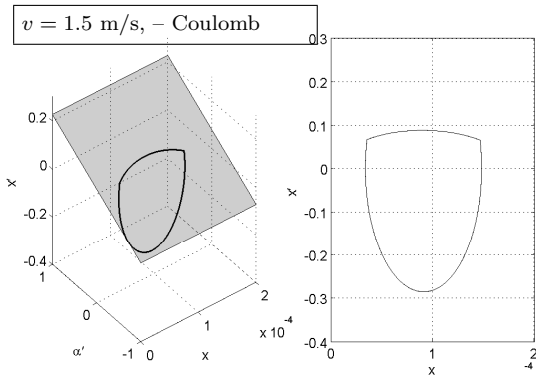


Figure 5:

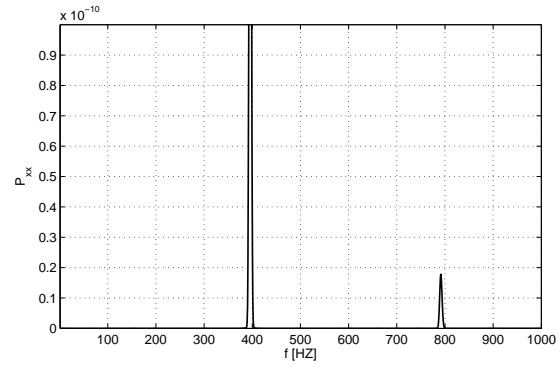


Figure 6:

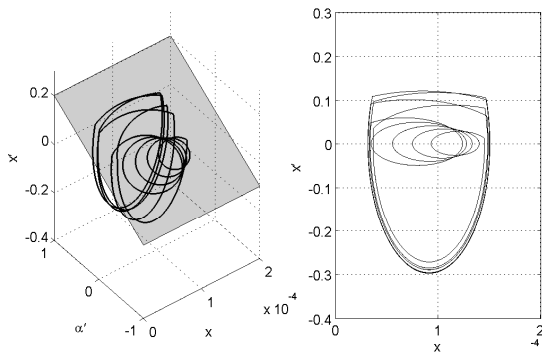


Figure 7:

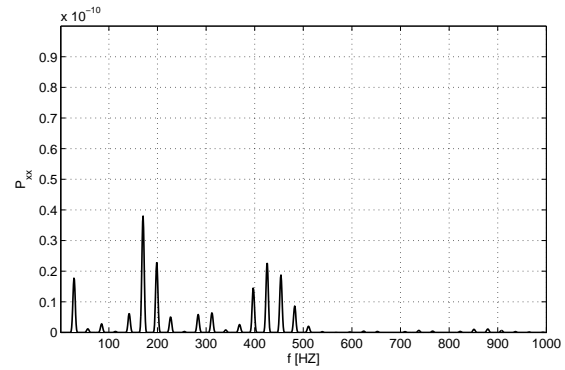


Figure 8:

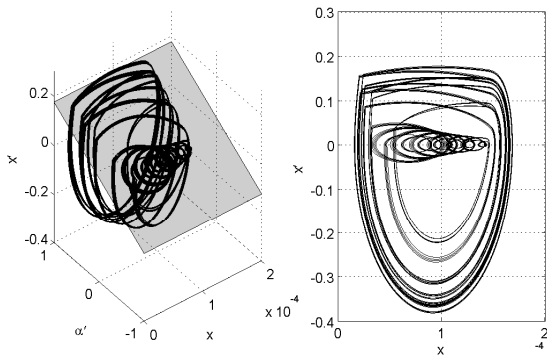


Figure 9:

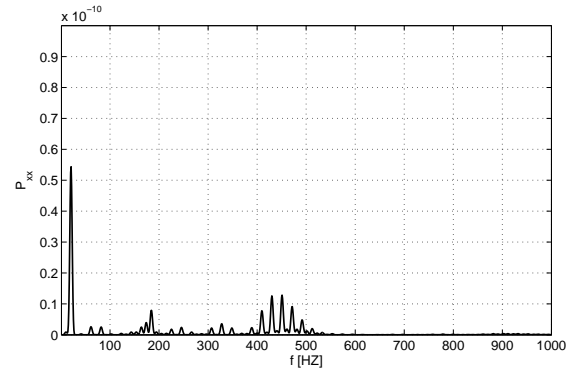


Figure 10:

Figure 11 and 12 show spectral power density plots of the pads' motion x for two different driving velocities $v_{car} = 0.2 \text{ m/s}$ and $v_{car} = 0.1 \text{ m/s}$ and Coulomb friction (cf. figure 3 and 4); figure 11 shows the typical spectrum of a periodic limit cycle, while figure 12 suggests a periodic or quasiperiodic limit cycle. While for moderate velocities (fig. 11) the spectral behaviour of the 2-DOF system is quite similar to that of the 1-DOF model it's obvious that the special limit cycle arising for very low velocities (fig. 11) causes pronounced low frequent spectral contents.

To get a qualitative overview over the spectrum in the low frequency band de-

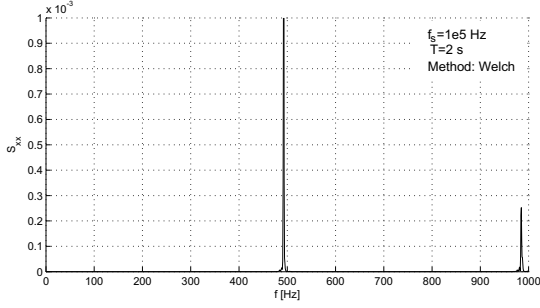


Figure 11: Spectral power density for limit cycle at $v_{car} = 2\text{m/s}$ (cf. fig. 3) .

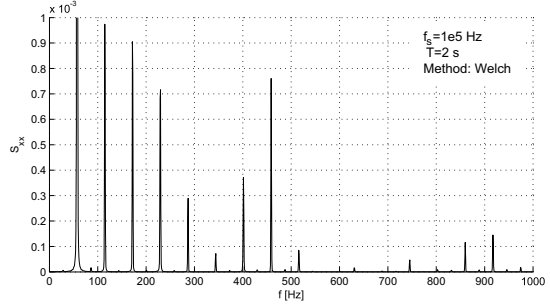


Figure 12: Spectral power density for limit cycle at $v_{car} = 1\text{m/s}$ (cf. fig. 4).

pending on the systems parameters figures 13 and 14 show the ratio

$$r_{200} = \frac{\int_0^{200} S_{XX}(f)df}{\int_0^{f_{max}} S_{XX}(f)df} \quad (10)$$

of the power in the interesting spectral band $f < 200$ Hz relative to the overall power in the entire simulated frequency band ($f_{max} = 1/2 \cdot 10^5$ Hz). Furthermore the center of gravity of the area below the spectral density is plotted to characterize where the emphasize of the spectral power is situated.

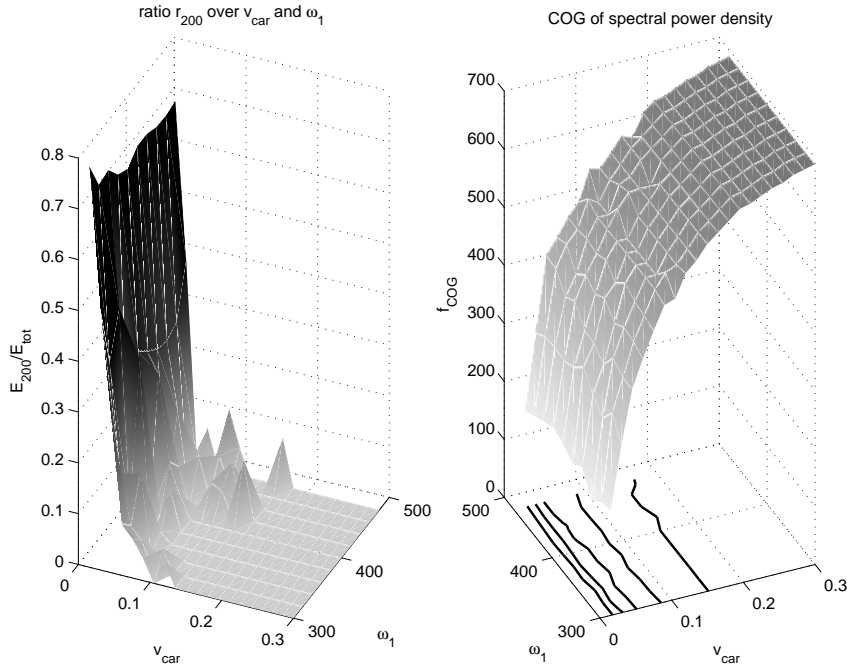


Figure 13:

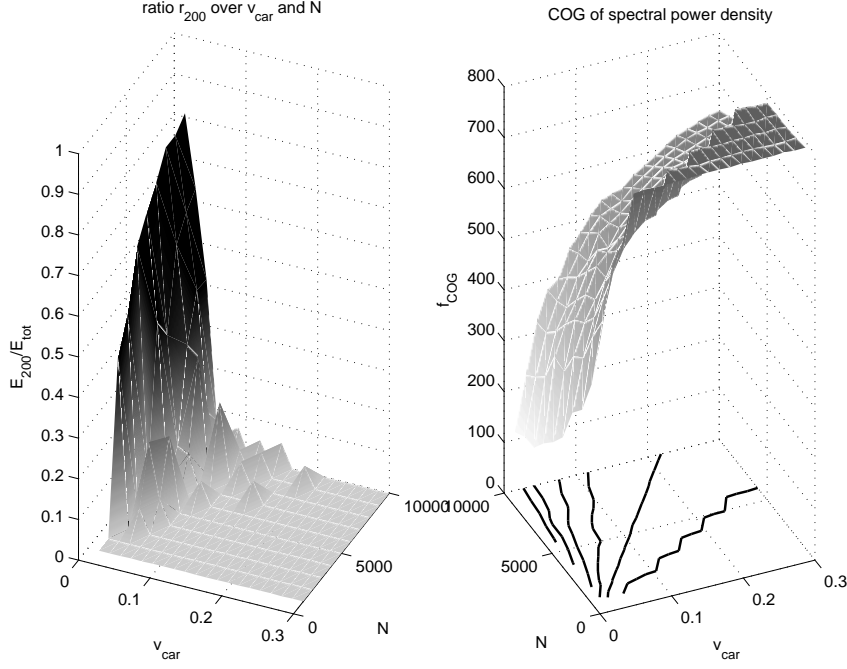


Figure 14:

4 Linear stability of the steady state

Taylor expansion and linearization about the steady state leads with the abbreviation $\vec{\eta} = \vec{z} - \vec{z}_0$ to the variational equations

$$\dot{\eta} = \mathbf{A}\eta + \vec{b}N \frac{\partial R}{\partial v_{rel}} \mathbf{w}^T \eta \quad \mathbf{w} = [0 \ 0 \ b \ -1] \quad (11)$$

$$= \underbrace{\left[\mathbf{A} + \vec{b}N \frac{\partial R}{\partial v_{rel}} \mathbf{w}^T \right]}_{=\mathbf{A}^*} \eta. \quad (12)$$

The state state's stability is studied using the Hurwitz criterion to check if positive realparts of the eigenvalues of \mathbf{A}^* appear. The characteristic polynomial of (12) has the form $P(\lambda) = A_0\lambda^4 + A_1\lambda^3 + A_2\lambda^2 + A_3\lambda + A_4$ with the coefficients

$$\begin{pmatrix} A_0 \\ A_1 \\ A_2 \\ A_3 \\ A_4 \end{pmatrix} = \begin{pmatrix} 1 \\ (J\rho N + 2\rho N b^2 m + 2D_1 \omega_1 Jm + 2JD_2 \omega_2 m) / Jm \\ (4\rho N b^2 D_2 \omega_2 m + \omega_1^2 Jm + 4D_1 \omega_1 JD_2 \omega_2 m + 2D_1 \omega_1 J\rho N + \omega_2^2 mJ) / Jm \\ (\omega_1^2 J\rho N + 2\omega_2^2 m\rho N b^2 + 2\omega_1^2 JD_2 \omega_2 m + 2\omega_2^2 mD_1 \omega_1 J) / Jm \\ \omega_1^2 \omega_2^2 \end{pmatrix} \quad (13)$$

With H_k denoting the k -th subdeterminant of the Hurwitz matrix H , the Hurwitz criterion in the modification of Lienhard/Chipart assures asymptotic stability if the following conditions are fulfilled:

$$I: \quad A_0 > 0$$

$$\begin{aligned}
II : & \quad H_1 = A_1 > 0 \\
III : & \quad A_2 > 0 \\
IV : & \quad H_3 = A_1 A_2 A_3 - A_0 A_3^2 - A_1^2 A_2 > 0 \\
V : & \quad A_4 > 0.
\end{aligned} \tag{14}$$

While condition I and V are priori fulfilled, conditions II - IV are crucial and determine the system behaviour and have to be checked. Figure 15 shows the stability

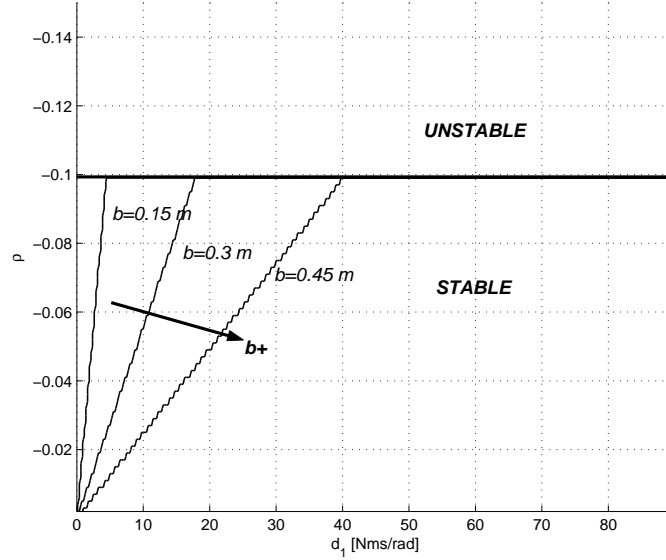


Figure 15: Influence of parameter b over tyre damping d_1 and friction slope $\rho = \left. \frac{\partial \mu}{\partial v_{rel}} \right|_0$.

border defined by the above stability conditions over the tyre damping d_1 and the friction slope $\rho = \left. \frac{\partial \mu}{\partial v_{rel}} \right|_0$ for constant parameters $J, m, \omega_1, \omega_2, D_2, r_{rad}$. It is found, that as well as in the one dimensional model a negative friction slope destabilizes the steady state. The stability border for the 1-DOF system is demarked by the bold line at $\rho = -0.1$. Furthermore its obvious that the stability of the 2-DOF system depends on the tyre damping d_1 and the the radius b of the pads' contact point.

Since linear models of real tyres have damping parameters of approximately $d_1 \approx 50$ Nms/rad and contact point radii of about $b \approx 0.15$ m the tyre has no effect on the destabilization of the steady state. Therefore within the parameter regime valid for car tyres the stability border can be calculated using the condition of the 1-DOF system.

If at least one of the realparts of the eigenvalues gets positive, the steady state turns from a stable to an unstable (repelling) singular point in the phase space and therefore the system will move towards the limit cycle. While the system with Coulomb friction can only reach the limit cycle if the initial condition provoke a motion leading to the sticking plane \mathcal{H} and will otherwise end up in the steady state, the Stribeck characteristic can even lead motions starting in the steady state lead into the limit cycle.

5 Outlook

References

- [1] P.W.A. Zegelaar; H.B. Pacejka: Dynamic Tyre Responses to Brake Torque Variations, in: *Tyre Models for Vehicle Dynamic Analysis*, suppl. to: *Vehicle System Dynamics*, Vol.27 (edited by Böhm, F.; Willumeit, H.-P.), Swets& Zeitlinger B.V., Lisse, Netherlands, 1997
- [2] Ch. Schmalfuß: Theoretische und experimentelle Untersuchung von Scheibenbremsen, *VDI Fortschrittbericht*, Reihe 12, Nr. 494, 2002
- [3] U. von Wagner, T. Jearsiripongkul, et.al.: Brake Squeal: Modelling and Experiments, *VDI Bericht*, Nr. 1749, S. 173-186, 2003
- [4] K. Magnus, K. Popp: Schwingungen, *Leitfäden der angewandten Mathematik*, Bd. 3, Teubner Verlag, Stuttgart, 2002

Wolfgang Seemann, Hartmut Hetzler

Universität Karlsruhe (TH) – Institut für Technische Mechanik – 76128 Karlsruhe, Germany